

Deposition and characterization of $\text{YBa}_2\text{Cu}_3\text{O}_{7-\delta}/\text{LaMnO}_3/\text{MgO}/\text{TiN}$ heterostructures on Cu metal substrates for development of coated conductors

C. Cantoni, D.K. Christen, and M. Varela

Oak Ridge National Laboratory—Condensed Matter Science Division, Oak Ridge, Tennessee 37831

J.R. Thompson

Oak Ridge National Laboratory—Condensed Matter Science Division, Oak Ridge, Tennessee 37831 and Department of Physics, University of Tennessee, Knoxville, Tennessee 37996-1200

S.J. Pennycook

Oak Ridge National Laboratory—Condensed Matter Science Division, Oak Ridge, Tennessee 37831

E.D. Specht and A. Goyal^{a)}

Oak Ridge National Laboratory—Metals and Ceramics Division, Oak Ridge, Tennessee 37831

(Received 24 April 2003; accepted 8 July 2003)

In this paper a novel buffer layer architecture consisting of $\text{LaMnO}_3/\text{MgO}/\text{TiN}$ is proposed as a suitable structural and chemical template for the epitaxial growth of high-transition temperature (T_c) superconductors on Cu metal surfaces. Using techniques such as high-energy electron diffraction and scanning transmission electron microscopy, we present *in situ* and *ex situ* analyses of the buffer-layer and superconductor growth with focus on structural properties of the interfaces formed. While MgO is a good barrier to oxygen diffusion, we find that MgO alone is not a suitable buffer layer due to rapid Cu diffusion. Further, growth of MgO with a single epitaxy can be hindered by the presence of impurities such as S, which form strongly bonded superstructures on the metal surface. With the addition of a TiN layer as a barrier to Cu diffusion, oxide formation is suppressed, interfaces are clean, and a single cube-on-cube epitaxy is observed. While the Cu/TiN and TiN/MgO interfaces are rough, the MgO and LaMnO_3 layers planarize the material, leading to growth of smooth $\text{YBa}_2\text{Cu}_3\text{O}_{7-\delta}$ (YBCO). Residual strain in the YBCO film is 0.25% or less and does not lead to apparent cracking. The superconducting properties of the samples were investigated by electrical transport and magnetization measurements. For the first time, high critical current density (J_c) values are reported for YBCO films grown on (001) single-crystal and {100}<100> textured Cu surfaces without intervening metal coatings. J_c on single crystal-like substrates is as high as 3.5 MA/cm². Reduced J_c of approximately 1 MA/cm² on rolled Cu tapes is limited by damage to the tape surface during the rolling process.

I. INTRODUCTION

The development of a superconducting wire technology that is functional at liquid-nitrogen temperatures holds significant promise, thanks to the recent progress in the fabrication of meters-long biaxially textured coated conductors. Ultimately, the success of this technology will be determined by several key factors, including material and processing costs, robustness and reproducibility of the coatings, reliability of these conductors against

thermal transients, and limitation of energy losses introduced by operation in alternating current (ac). To date, Ni and Ni-alloy tapes have been used as flexible metal substrates on which appropriate buffer layers and ultimately the high-temperature superconductor (HTS) coating are deposited. However, in the future, more successful coated conductor architectures could involve different metal substrates and/or different buffer materials than those used today.

Recently, within the rolling-assisted biaxially textured substrate (RABiTS) technology,¹ pure Ni substrate tapes have been replaced by Ni-alloy tapes with small impurity content that offer improved mechanical properties and reduced ferromagnetism.^{2–11} Meters-long RABiTS

^{a)}This author was an editor of this journal during the review and decision stage. For the *JMR* policy on review and publication of manuscripts authored by editors, please refer to <http://www.mrs.org/publications/jmr/policy.html>.

conductors carrying more than 100 A/cm width of current at 77 K in a self-magnetic field are now fabricated on Ni-3%W and Ni-5%W alloys.¹² Despite their much-reduced Curie temperature and hysteretic losses, these alloys still add to the overall ferromagnetic (FM) losses associated with a single YBa₂Cu₃O_{7- δ} (YBCO) wire. Moreover, because of their increased reactivity toward oxygen with respect to pure Ni, Ni protective films with micrometer thickness are regularly deposited on the alloy tape prior to buffer-layer deposition,¹³ further contributing to the total wire ac losses.

Using Cu-based tapes as the metal substrate would address several drawbacks of the present Ni-alloy tapes. Pure Cu can be thermomechanically processed to obtain a very sharp cube texture with a true in-plane full width at half-maximum (FWHM) of nearly 4°. In addition, Cu, which is only slightly diamagnetic, does not contribute to hysteretic ac losses. Cu-based tapes will have significantly greater thermal conductivity than Ni-based tapes, and, because the Cu industry is so well established, Cu tapes may be potentially less expensive than Ni tapes. Copper, in its pure form or strengthened by opportune metal additions or precipitates, has another important advantage over Ni alloys: low electric resistivity (ρ [Cu] = 0.2 $\mu\Omega$ cm; ρ [Ni-3%W] = 20 $\mu\Omega$ cm at 77 K). This property is required, in practical applications, if the substrate is to provide stabilization to the HTS coating in an over-current situation. In the presence of a crack or other local defect in the superconducting layer, or in response to an unexpected increase in temperature, the current in the YBCO film can be shunted to the 50- μ m-thick metal substrate, with consequent reduction of the dissipated power below a certain operational critical level. This scenario requires development of a conductive buffer layer that would properly couple the HTS layer to the underlying Cu substrate. Alternatively, if a high-resistivity Ni-alloy tape is chosen as substrate, cryogenic and/or adiabatic stabilization can be achieved only by depositing a thick Cu cap layer on the YBCO film. This situation, however, has the disadvantage of decreasing considerably the engineering critical current density (J_E ; current/total cross section) of the coated conductor, which is a critical parameter in device design.^{14,15}

Until now, experiments on the growth of multilayer structures consisting of epitaxially oriented oxide buffer layers and YBCO films on Cu (001) substrates have not produced successful results. This outcome is not surprising considering the poor resistance of Cu to oxidation compared to Ni.

In systems like Cu and Ni, the prevailing metal oxide (Cu₂O, CuO, NiO) growth occurs at the oxide-gas interface and is governed by outward metal cation diffusion through oxide lattice sites or defects.¹⁶⁻¹⁸ A typical RABiT substrate is composed of a combination of CeO₂,

Y₂O₃, and yttria-stabilized zirconia (YSZ) buffer layers on the metal tape. At the temperatures necessary to process YBCO, these oxides are poor barriers to oxygen diffusion, and oxygen inevitably diffuses to the metal interface causing formation of some NiO. However, because the buffer layers (and the native nickel oxide) are suitable barriers for Ni diffusion, Ni oxidation is contained in a thin and often epitaxial layer at the metal/buffer interface and is not detrimental to the YBCO layer. Lattice diffusivities of Cu ions in Cu₂O and oxides in general are much higher than in the case of Ni.^{18,19} For this reason, Cu oxide is less self-limiting than NiO at high temperatures, and preventing eruptions of CuO/Cu₂O during buffer-layer and YBCO growth presents a major challenge.

Reports of high critical current density (J_c) YBCO films on Cu substrates have been limited to the case in which a protective Ni layer in excess of 1- μ m thickness is deposited on the substrate prior to buffer-layer deposition.²⁰ The sufficiently thick Ni layer adequately prevented the transient Cu diffusion to the surface, enabling deposition of buffer layers and YBCO at typical conditions used for Ni tapes. Because of its ferromagnetic hysteresis, however, the Ni film caused energy losses in ac response that were estimated to be comparable with those measured for Ni-alloy tapes such as Ni-5%W and Ni-7%Cr.³ Although Ni-coated Cu tapes may be an interesting approach in applications that involve intense ac fields, a totally nonmagnetic substrate is most desirable. The deposition of suitable buffer layers directly on the Cu surface is a challenging problem. However, the study of Cu/buffer layer interfaces and their modification during YBCO deposition is required to assess the feasibility of Cu-based RABiTS. In addition, studies of deposition of buffer layers and high-transition temperature (T_c) cuprates on Cu surfaces contribute to a fundamental understanding of metal oxide interfaces in general.

In this paper, we investigate the issues associated with the development of buffer and superconducting layers directly on Cu substrates. These issues include the poor Cu oxidation resistance, high Cu thermal expansion, and surface sulfur-mediated buffer-layer epitaxy. We identify a new buffer-layer architecture, LaMnO₃/MgO/TiN, which acts as a suitable barrier to both Cu and O diffusion during the YBCO deposition process. The combined use of TiN and MgO is necessary to avoid detrimental Cu oxidation during the YBCO growth. In fact, TiN blocks outward Cu diffusion through the oxide buffer layers to the growing YBCO film, while MgO acts as a good barrier to inward oxygen diffusion, impeding TiN decomposition (into Ti_xO_y and N₂) and keeping TiN/MgO and Cu/TiN interfaces clean. We report for the first time J_c s approaching 4 MA/cm² at 77 K in self-field on (001) single-crystal-like Cu surfaces and 1 MA/cm² on biaxially textured Cu tapes. All the samples discussed

in this paper are entirely nonferromagnetic and no Ni overlayers were used to passivate the Cu surface. In all cases the crystal structure of the buffer layers was monitored during pulsed laser deposition (PLD) by reflection high-energy electron diffraction (RHEED) and analyzed, after growth, by x-ray diffraction (XRD). On selected samples, careful high-resolution scanning transmission electron microscopy (STEM) analysis was performed, with particular focus on the interfaces of the multilayered structure, to evaluate possible interdiffusion or chemical reaction between different layers.

II. EXPERIMENTAL

The Cu substrates used for this study include Cu (001) single crystals, Cu (001) epitaxial films deposited on (001) MgO or (001) SrTiO₃ (STO) single crystals, and {100}<100> textured Cu tapes. The Cu single crystals were cut in $8 \times 6 \times 1.5$ mm³ pieces and electropolished in a 1:1 solution of phosphoric acid and water. Although the surface of these samples was optically rough, streaks consistent with a (001) Cu surface were observed in the RHEED patterns at deposition conditions. The Cu films, 1 to 3 μm thick, were deposited by sputtering or e-beam evaporation at a temperature of 400 °C and showed RHEED patterns expected for a Cu (001) surface. The Cu biaxially textured substrates were obtained by cold-rolling commercial Cu tape of 99.99% purity and annealing it at 800 °C in a background pressure of 10⁻⁸ torr for 1 h. XRD measurements showed full cube texture with a FWHM for ω- and φ-scans of about 6°. RHEED observations up to temperatures of 800 °C in high vacuum showed that the surface of these samples was covered by a few-Å-thick polycrystalline film, most likely Cu_xO formed during the texturing anneal. This layer was removed by sputter-cleaning the surface with an Ar⁺ beam with energy of 500 eV for 4 to 6 min.

All the oxide buffer layers discussed in this paper were grown in an ultrahigh vacuum (UHV) PLD chamber equipped with a load lock for loading samples and targets, a RHEED system, a residual gas analyzer, and a Kauffman-type ion source. The laser used for ablating target materials was a KrF excimer laser with a power of 150 W and a wavelength of 248 nm. The laser fluence varied between 4 and 5 J/cm², and the repetition rate varied between 10 and 20 Hz.

III. SULFUR SUPERSTRUCTURES ON (100) Cu

In previous publications, we have documented that a centered 2 × 2 superstructure, which forms by chemisorption of sulfur on the Ni and Ni-alloy surface, promotes epitaxial nucleation and growth of oxide buffer layers with perovskite, bixbyite, and fluorite crystal structures.^{21,22} Exposing the metal surface to low partial

pressures of H₂S allows control of the coverage of the sulfur superstructure prior to buffer-layer deposition and prevents occurrence of misoriented domains in the seed buffer layer. Using this approach, we were able to achieve very high reproducibility and uniformity in the buffer layer texture over meters-long Ni tapes processed continuously.²³

We found that an ordered sulfur template is also necessary on a Cu (001) surface to obtain epitaxial growth of oxides like STO or CeO₂, which are often used as seed layers in RABiTS. However, the S atoms interact quite differently with the surface Cu atoms than they do with the Ni surface atoms. As documented in previous studies by others, the interaction between the chemisorbed S atoms on Cu is less attractive than in Ni, and at low temperatures (25 °C < T < 200 °C) the S saturation coverage on Cu is half the value found for Ni. In this case, adsorption of S atoms by exposure of the Cu surface to H₂S leads to the formation of a *p* (2 × 2) superstructure rather than a *c* (2 × 2).²⁴ Higher levels of S adsorption on Cu have been reported in some cases, but they did not lead to the formation of ordered and stable 2 × 2 superstructures.^{25–27} We observed that the *p* (2 × 2) superstructure grown on Cu using H₂S at room temperature was inadequate for the epitaxial growth of cubic materials because it was not stable once the sample was heated at temperatures above 225 °C, producing more complex and often disordered RHEED patterns. However, in cases in which the Cu samples incidentally contained bulk sulfur impurities, a stable *p* (2 × 2) RHEED pattern was observed as a result of outward S segregation when the sample was heated at typical buffer-layer deposition temperatures (*T* ~ 600 °C), as shown by the RHEED pattern of Fig. 1. The S-containing Cu samples were obtained by depositing 3-μm-thick Cu films on STO (001) and MgO (001) substrates by e-beam evaporation. The source of S present in the films was likely the evaporated Cu metal itself (S is a common impurity in many metals) or the chamber background environment. Auger electron spectroscopy analysis detected presence of S on the surface of these samples after heating above 400 °C in UHV. The coverage of the S layer was estimated to be nearly 0.25 ML, equal to the coverage of a complete *p* (2 × 2) layer. Figure 2 shows a comparison of RHEED patterns and (111) φ-scans acquired for STO films deposited on the *p* (2 × 2) template and on a clean (001) Cu film, respectively, using MgO as substrate. The RHEED patterns were acquired after the first approximately 50 PLD shots, corresponding to a film thickness of 5 to 10 Å, and the XRD φ-scans were acquired after the deposition of a nearly 500-Å-thick film was completed. The figure shows that deposition on the *p* (2 × 2) template produced an epitaxial (001) STO film [Fig. 2(a)], while deposition on the clean Cu surface results in additional 45° in-plane rotated STO domains

[Fig. 2(b)]. Similar results were obtained with CeO₂ films. In this case, growth of CeO₂ on a clean Cu surface resulted in films with additional (111) oriented and 45° rotated crystal domains.

These experiments show that growth of a standard oxide buffer-layer architecture such as CeO₂/YSZ/CeO₂ on Cu is possible provided that a $p(2 \times 2)$ S superstructure is present on the Cu surface. However, growth and control of such S superstructure on the Cu surface is not

straightforward. In addition, because of the high diffusivity of Cu and oxygen through CeO₂ and YSZ, the standard buffer layer architecture proved unsuitable for subsequent YBCO deposition, leading to pervasive Cu oxidation and film spallation.

IV. CHOICE OF BUFFER MATERIALS FOR CU-BASED SUBSTRATES

Among the possible oxides used today in coated conductor technologies, MgO is certainly a good candidate as a barrier layer in buffer-layer architectures intended for Cu. Previous O¹⁸ transport studies indicate that the oxygen diffusion coefficient of MgO at 800 °C is roughly 10⁻²⁰ cm²/s, nearly 13 orders of magnitude smaller than that of YSZ at the same temperature.^{28,29} As MgO is known to have poor structural compatibility with YBCO, a MgO buffer layer should be capped with an oxide better matched to the YBCO lattice. Among several perovskite materials known to grow epitaxially on (001) MgO and to have a good lattice match with YBCO, we chose LaMnO₃ (LMO) as the cap layer because of the wide window of deposition conditions for single-oriented (100) films. To test the MgO/LMO architecture, we grew both oxide layers *in situ* on (100) Cu films previously deposited on (100) STO single crystals. As shown by recent studies, MgO and other oxides with the NaCl crystal structure are different from other classes of buffer layers because they grow epitaxially on clean face-centered-cubic (fcc) metal surfaces and show deviations

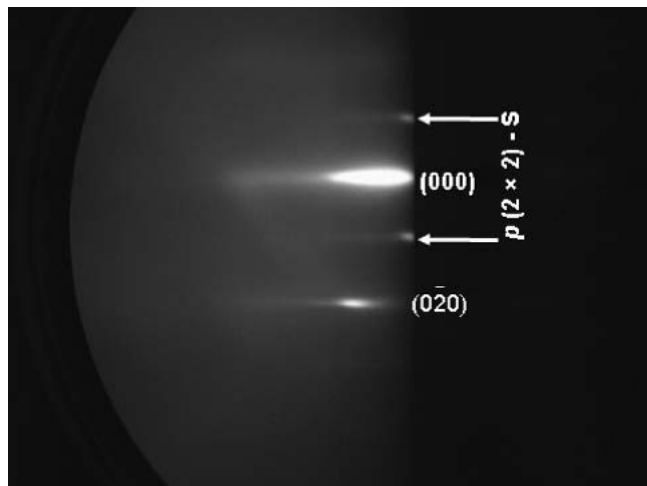


FIG. 1. RHEED pattern acquired from a Cu film epitaxially deposited on STO single crystal by e-beam evaporation, acquired after the sample was heated to 600 °C in vacuum. The arrows indicate extra reflection from a $p(2 \times 2)$ -sulfur superstructure. The electron beam is parallel to the film [100].

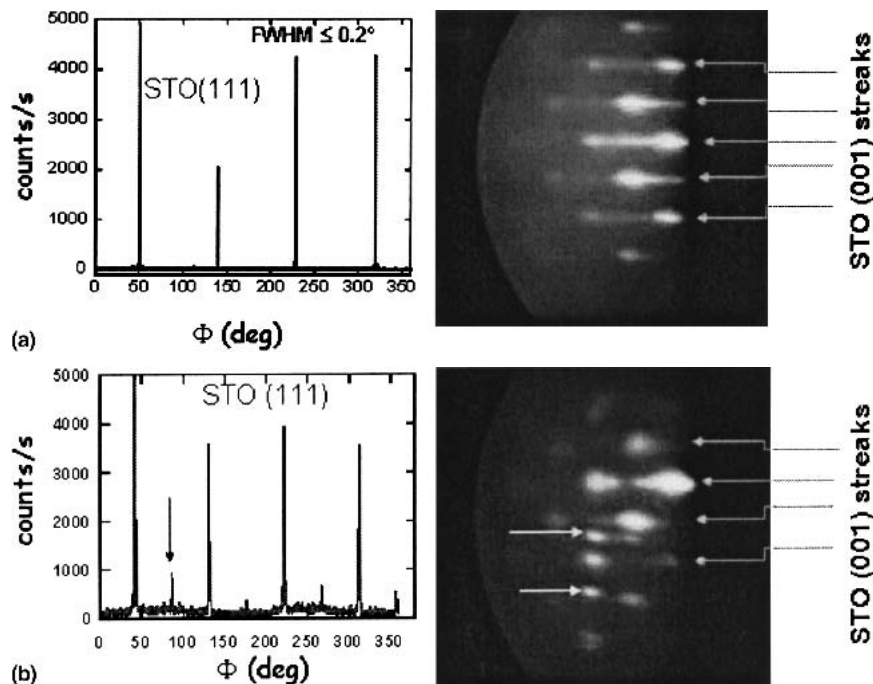


FIG. 2. XRD ϕ -scans of the (111) peak and nucleation RHEED patterns obtained from STO films deposited on (a) a Cu film on MgO single crystal with $p(2 \times 2)$ -S superstructure, and (b) a Cu film on MgO single crystal with sulfur-free surface.

from epitaxy when an S superstructure is present on the metal surface.³⁰ Nevertheless, even when using sulfur-free Cu samples, we were not able to grow single-oriented MgO layers directly on the Cu surface. Consequently, the MgO films were deposited on a thin (~50 Å) STO nucleation layer that had been previously deposited *in situ* on the $p(2 \times 2)$ S superstructure of the e-beam deposited Cu film. The MgO films were grown at a temperature of 500 °C and an oxygen partial pressure of 1×10^{-6} torr, using a stoichiometric ceramic target, with a thickness of nearly 200 nm. The LMO films, 300 nm thick, were deposited at a temperature of 600 °C to 620 °C in a H₂O background with a partial pressure of 3 to 6 mtorr. Figure 3 shows a RHEED pattern of the as-deposited MgO and LMO films with the e-beam directed along the substrate [100]. The position of the diffracted beams indicates that both films have single (100) orientation and have grown with a cube-on-cube epitaxial relationship. The well defined and elongated streaks indicate that the film surface is atomically smooth and growth had proceeded in a two-dimensional fashion. Combined XRD and energy dispersive x-ray measurements showed no evidence of Cu oxide in these films. The as-grown films were subsequently subjected to a furnace heat treatment that reproduced typical YBCO growth conditions. The anneal lasted 20 min and was conducted in flowing Ar with an oxygen partial pressure of 200 mtorr at a temperature of 740 °C. After this procedure the films looked rough and dull. Shown in Fig. 4 are the optical micrographs of one of these films before and after the heat treatment. EDX and XRD measurements conducted on the annealed films indicated that the particles present on the surface were Cu₂O outgrowths. Cu oxidation in this case had not caused blistering or spallation of the buffer layers, as is usually observed when metal oxide growth occurs at the metal/buffer-layer interface. This observation suggested that Cu had diffused from the base Cu film through the MgO and LMO layers and oxidized in proximity of the surface. In other words, the MgO film (as well as the LMO cap) did not effectively block Cu outward diffusion. The lack of an effective Cu diffusion barrier in the MgO/LMO architecture prevented the growth of high- J_c YBCO films on these samples.

In search of a suitable Cu diffusion barrier, we considered the use of nitrides, which are known to block diffusion of Cu into Si in semiconductor devices and have been explored as buffer layers for Ni-based substrates.³¹ TiN is one of the most widely investigated barrier materials in Cu metallization for integrated circuit technology.³² In addition, TiN is a good electrical conductor ($\rho = 20$ to $30 \mu\Omega$ cm) and is widely used as a wear-resistive coating for tools because of its high mechanical toughness. Mechanical strength is a desirable property to prevent cracking in buffer layers intended for

RABiTS, and electrical conductivity is necessary, as mentioned previously, to ultimately use the metal substrate as a current shunt for stabilization during transient loss of superconductivity. TiN is also very compatible structurally with MgO, having the same rocksalt crystal structure and a lattice mismatch with MgO of only 0.5%.

V. RESULTS ON (001) Cu FILMS

Fully (100)-oriented, epitaxial TiN films were grown by PLD on the sulfur-free Cu film substrates using a TiN target in a nitrogen background pressure of 3.0 to 10×10^{-5} torr and a substrate temperature of 580 °C. The film nucleation and growth was monitored by RHEED, and a cube-on-cube epitaxial relationship was observed between the Cu substrate and TiN film. After a nearly 200-nm-thick TiN film was grown, the nitrogen was

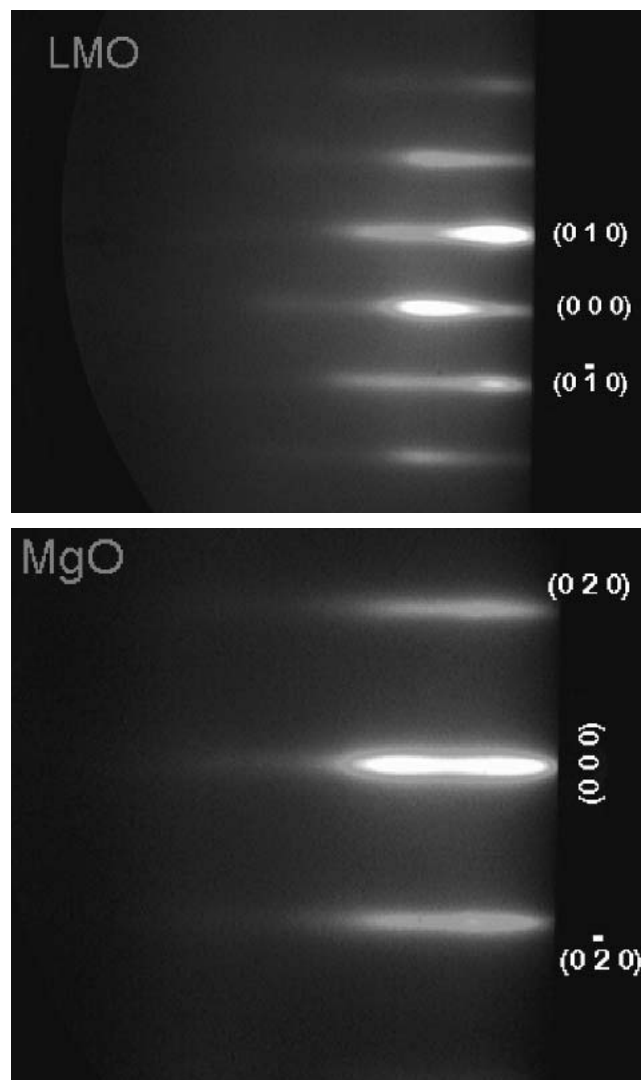
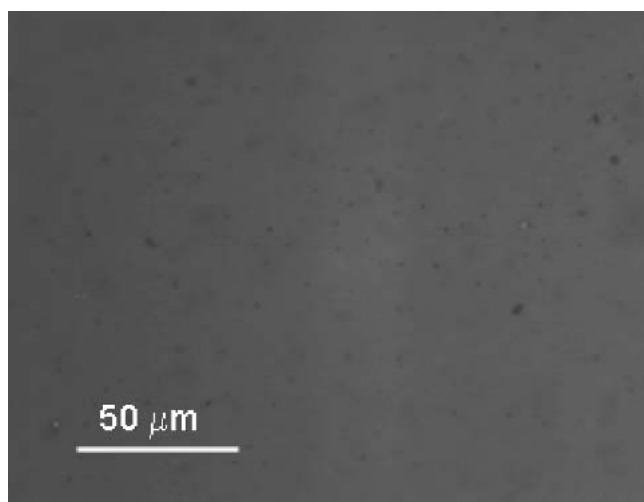


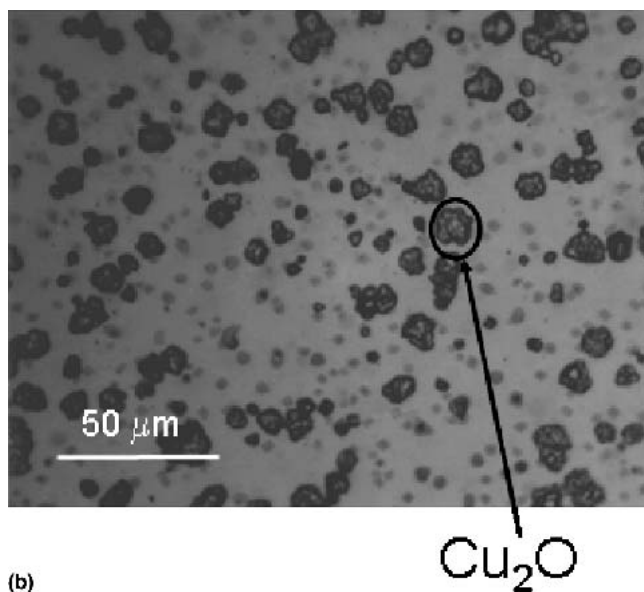
FIG. 3. RHEED patterns of LMO and MgO epitaxial films deposited on a Cu film on single crystal STO. The electron beam is parallel to the substrate [100].

pumped out, the substrate temperature was increased to 600 °C, and oxygen was introduced in the chamber with a partial pressure of 0.8 to 1.0×10^{-5} torr for the growth of the MgO layer. At such oxygen pressure, the TiN RHEED pattern exhibited spots in addition to those typical of a clean (001) surface. Figure 5 shows the RHEED pattern produced by a clean TiN surface and that of a TiN film when exposed to the oxygen pressure and temperature just indicated. The latter suggests the presence of a 6×6 superstructure, likely formed by oxygen adatoms bonded on film surface lattice sites. This superstructure was stable at the deposition condition used for the MgO buffer layer, and fully (001) oriented MgO films could be grown on this surface. A high-resolution STEM image acquired with a high-angle annular dark-field detector

(HAADF) of the TiN/MgO interface (taken after the YBCO was deposited) is shown in Fig. 6 for the case where the Cu substrate is an epitaxial film deposited on single-crystal (001) MgO. These images were obtained in a VG Microscopes' HB501UX field-emission STEM operating at 120 kV equipped with a Nion aberration corrector with a field-emission gun and a parallel electron energy loss spectroscopy (EELS) detector. HAADF imaging, also known as Z-contrast, provides direct compositional contrast; therefore, the atoms with a larger Z number (Ti atoms) appear brighter in the micrograph, while those with a smaller Z number (Mg atoms)

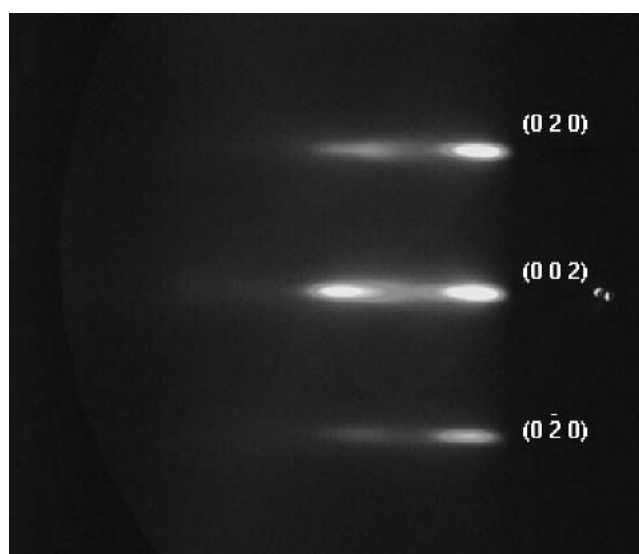


(a)

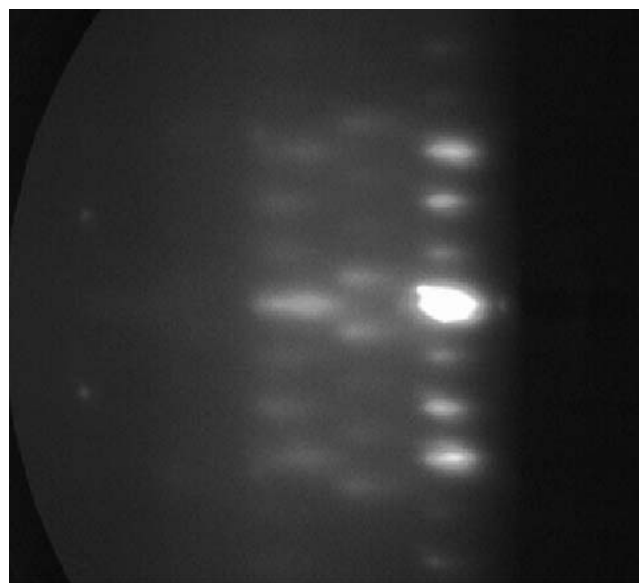


(b)

FIG. 4. Optical micrographs of the surface of a LMO/MgO/STO/Cu multilayer deposited on single-crystal STO (a) as grown and (b) after a heat treatment that reproduced typical conditions for YBCO growth.



(a)



(b)

FIG. 5. RHEED patterns of an epitaxial TiN film on (001) Cu (a) as deposited in a vacuum background and (b) when exposed to an oxygen partial pressure of 8×10^{-6} torr at a temperature of 600 °C.

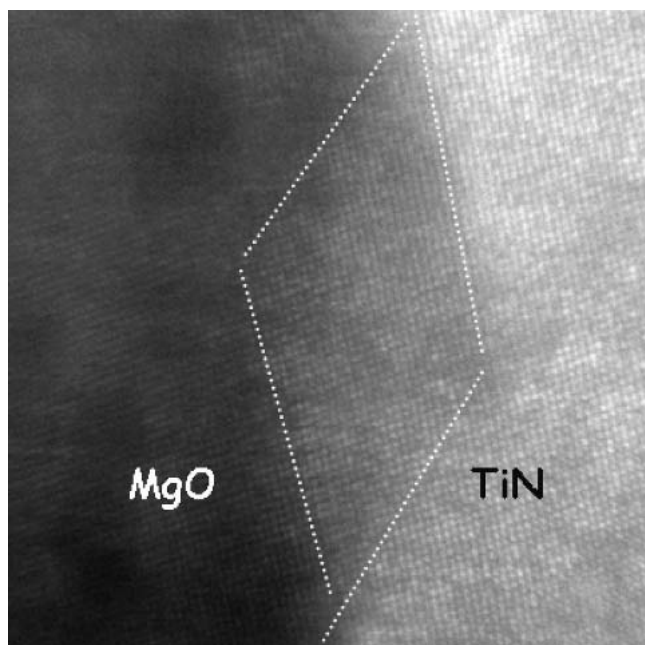


FIG. 6. High-resolution STEM image acquired with a HAADF of the TiN/MgO interface in a YBCO/LMO/MgO/TiN/Cu multilayer on single-crystal MgO.

appear darker. Light elements such as O and/or N are not visible with the current resolution of the microscope, estimated to be of 0.12 nm.

The interface appears jagged and rough with some overlap of the two materials in the direction parallel to the electron beam, which leads to the intermediate shade of gray visible in the middle of the image. Despite the evident roughness, this figure shows a perfect epitaxial relationship between the two materials and a very clean interface. In fact, given the similarity of the two crystal structures, the two compounds could not be identified without the contrast associated with their different Z values. The absence of chemical reaction at the TiN/MgO interface is consistent with thermodynamic data of free energy of formation for MgO and TiO, which indicate higher stability of the former oxide as compared to the latter. The formation of MgO is thus favored over the formation of TiO, and the O adatoms initially present on the TiN surface at the time the MgO deposition starts are likely incorporated in the growing MgO film.

Once a 100-nm-thick MgO film was grown, an additional LMO cap layer was deposited *in situ* using the conditions indicated in the first paragraph of this section. The RHEED patterns for the MgO and LMO films showed nice streaks indicative of two-dimensional film growth and were very similar to those shown in Fig. 3. High-resolution XRD ϕ and ω -scans of the LMO films [MgO and TiN films had reflections overlapping with the MgO (001) substrate] showed a certain broadening in the crystal structure of the buffer layers as compared

to the Cu epitaxial film. In fact, the (002) ω -scans FWHM were 1.47° and 0.184° for the LMO and Cu films, respectively. The corresponding values for the (111) ϕ -scans were 2.56° and 0.227°. A 180-nm-thick YBCO film was subsequently deposited on the LMO cap in a second PLD chamber at usual deposition conditions reported elsewhere.³³ The FWHM values for out-of-plane and in-plane alignment were in this case 1.03° [(005) ω -scan], and 2.54° [(115) ϕ -scan], respectively. Figure 7 shows the critical current density of the YBCO film measured by electrical transport as a function of the applied magnetic field at 77 K. The thickness of the YBCO film was measured by Rutherford backscattering spectroscopy and the corresponding J_c in self-field was 3.5 MA/cm². Such a value is comparable with those obtained on YBCO films deposited directly on single-crystal STO substrates. The behavior of J_c in field and the value of irreversibility field ($H_{irr} = 7$ T) are also typical of YBCO films on STO or LAO single crystals.

Figure 8(a) shows a low-magnification Z-contrast image of the multilayered structure LMO/MgO/TiN grown on the Cu film on MgO single crystal after deposition of the YBCO top film. All the interfaces shown appear clean and there is no evidence of detrimental reactions or interdiffusion between the different layers. Further, oxygen presence in the Cu/TiN interface was not detected from EELS measurements. The Cu/TiN and TiN/MgO interfaces look rather wavy and rough. Such roughness likely originates at the Cu film surface and is retained in the growing TiN film, as suggested by atomic force microscopy (AFM) imaging of as-grown sputtered Cu films that show an average roughness of 9 nm over areas of 12 × 12 μm^2 . Additional roughening of the TiN film could also result from the different thermal expansion of the two materials [$(\alpha_{\text{TiN}} - \alpha_{\text{Cu}})/\alpha_{\text{Cu}} = 48\%$].

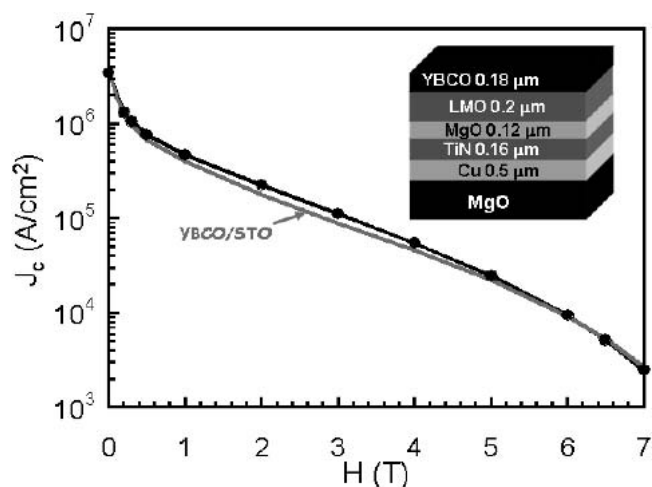
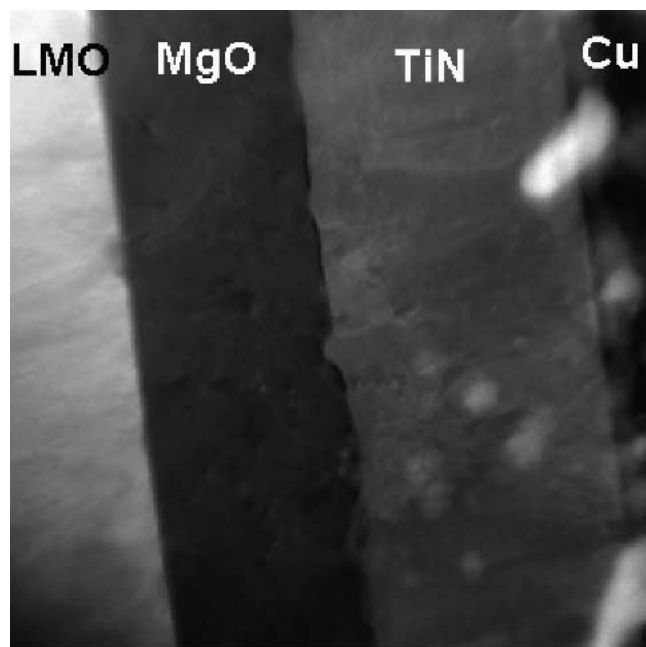
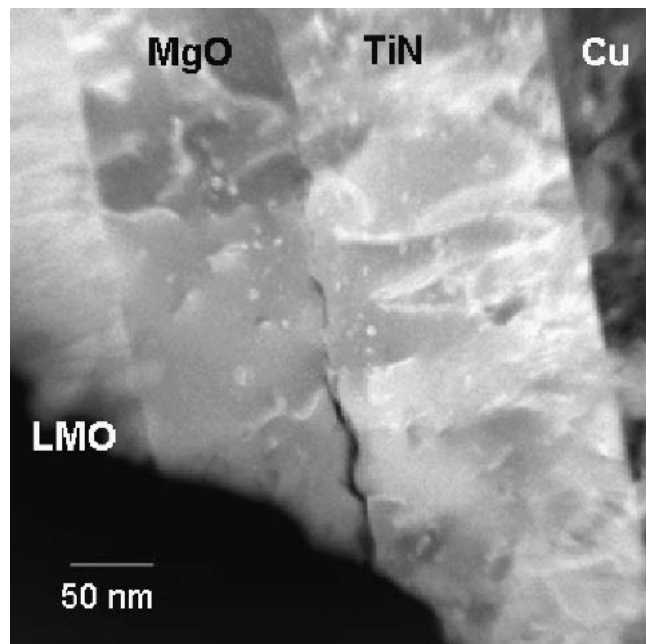


FIG. 7. Critical current density versus applied magnetic field for a YBCO film deposited on LMO/MgO/TiN/Cu/MgO (crystal) (black line and dots), and a typical YBCO film deposited on single-crystal STO (gray line). Both measurements were performed at 77 K.



(a)



(b)

FIG. 8. STEM image of a YBCO/LMO/MgO/TiN/Cu multilayer structure on MgO single crystal acquired with (a) HAADF and (b) LAADF.

The subsequent MgO/LMO and LMO/YBCO interfaces appear smooth and straight, suggesting that the MgO film has overgrown the rough features of the TiN film, planarizing the film/vacuum interface. In Fig. 8(b) the same region as in Fig. 8(a) is observed through the low-angle annular dark-field detector (LAADF), producing an image more sensitive to strain, misfit dislocations, and structural defects in general.³⁴ From this figure it is

evident that the TiN film is the most defective buffer layer in the entire heterostructure. However, strain and dislocation density decrease progressively as a function of film thickness and are greatly reduced in the MgO layer, ultimately leading to a high-quality LMO film, in which the only visible transmission electron microscopy (TEM) feature is a columnar grain structure that is typical of many perovskites grown by PLD. The ordered LMO microstructure results partially from a mechanism of strain relief by introduction of misfit dislocations occurring at the interface with MgO. As shown in the high-magnification Z-STEM image of Fig. 9 the large lattice mismatch between the two oxides is accommodated in the early stages of film nucleation with the introduction of disorder and dislocations in the very first atomic planes of LMO, leading to virtually unstrained growth of the rest of the film.

The lattice distortion of the different layers was investigated by high-resolution XRD measurements of the lattice constants of TiN, MgO, and YBCO for samples prepared on Cu films and on Cu crystals. The XRD data showed that in all samples the TiN unit cell is compressed in the basal plane and stretched along the *c* axis. The MgO film, instead, is subject to tensile strain in the basal plane and compressive strain along the substrate normal. In accord with the qualitative interpretation of Fig. 8(b), the TiN and MgO films are the most strained layer, while the lattice distortion decreases in the following layers. The out-of-plane and in-plane lattice parameters of TiN and MgO were calculated from (002) and (111) type reflections, which gave $(a - c)/a = -0.66\%$ for the TiN film and $(a - c)/a = 1.01\%$ for the MgO

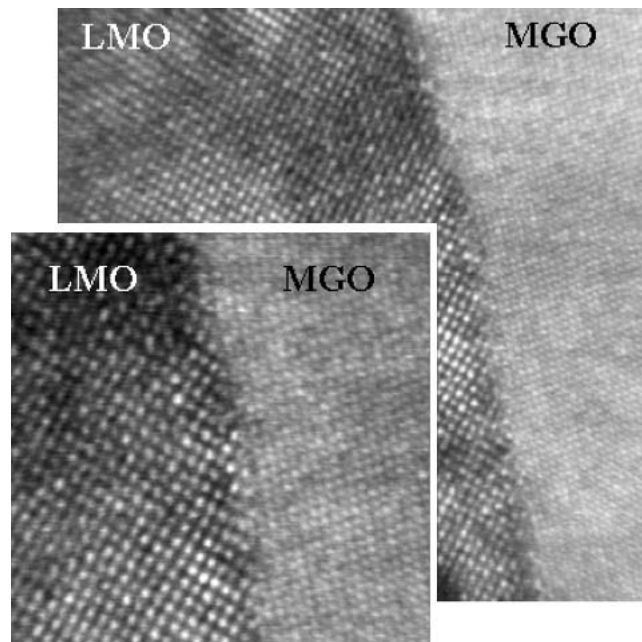


FIG. 9. High-resolution STEM micrograph of the LMO/MgO interface for the sample shown in Fig. 8.

film. The lattice constants were calculated using an YBCO/LMO/MgO/TiN multilayer identical to the one in Fig. 8, grown on a STO substrate to avoid overlapping of films and substrate reflections. However, because of their very close lattice match, TiN and MgO (111) reflections overlapped, introducing ambiguity in the distinction of the two films. For this reason, an additional sample composed of only a TiN/Cu film on STO substrate was used to sort out the calculated lattice parameters and unambiguously individuate those corresponding to the TiN film. The YBCO lattice parameters for the sample in Fig. 8 were calculated from the (113), (005), and (006) reflections and were $(a + b)/2 = 3.850$ and $c = 11.670$, the same as for bulk YBCO. The YBCO lattice was not strained for all the samples deposited on the Cu films, which had a thickness of nearly 1 μm .

A high-magnification close-up of the YBCO/LMO interface is shown in Fig. 10. The interface is flat and coherent with one-unit-cell-high steps occasionally found. Because of the compositional contrast, we can easily distinguish the different atomic planes of the YBCO lattice. The Cu–O chains are the least dense and lightest of the planes and therefore show up as the darkest atomic rows, while the brightest rows in the micrograph correspond to the Ba–O planes. A common defect of the YBCO lattice is the insertion of an extra Cu–O chain plane as indicated by the arrow in Fig. 10. This type of dislocation is often observed in YBCO epitaxial films and is also referred to as Y-248 intergrowth.³⁵ The position of the interface (indicated in Fig. 10 by a dashed line) was located analyzing intensity traces and

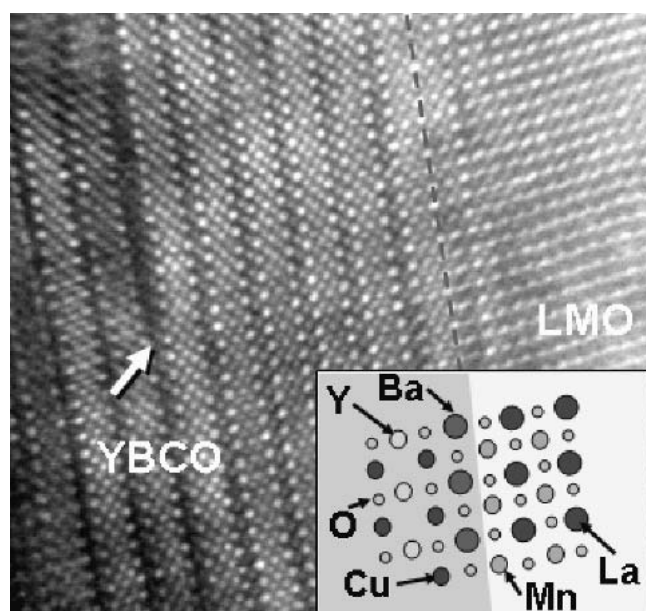


FIG. 10. High-resolution STEM image of the YBCO/LMO interface of the sample YBCO/LMO/MgO/TiN/Cu/MgO (crystal) shown with low magnification in Fig. 8 and corresponding atomic model (inset).

comparing them to those obtained on step-free, atomically flat LMO/YBCO superlattices.³⁶ No CuO chains were observed at the interface between YBCO and LMO, suggesting a structural interface model like the one shown in the inset of Fig. 10. In the samples we examined, the topmost atomic plane of the LMO film was a Mn–O plane, and the first YBCO plane to nucleate on the manganite was a Ba–O plane, followed by a CuO₂ plane, a Y plane, and another CuO₂ plane. In LMO, the MnO₂ and LaO atomic planes correspond to the B-plane and A-plane of a perovskite cell, respectively. The Ba–O plane in YBCO can also be regarded as a perovskite A-plane and is very similar structurally to the LaO plane in LMO. It is likely, thus, that the atomic arrangement we observed at the YBCO/LMO interface corresponds to minimum interface free energy.

VI. RESULTS ON (001) Cu CRYSTALS

As mentioned earlier, one of the concerns related to the use of a Cu-RABiT substrate is the large strain imposed by the substrate on the YBCO film during cooldown. In fact, the thermal expansion coefficient of Cu can be estimated as $18 \times 10^{-6} \text{ K}^{-1}$ in the temperature region of interest (the same quantity for Ni is $16 \times 10^{-6} \text{ K}^{-1}$). On the sole basis of the difference between Cu and YBCO thermal expansion ($\alpha_{\text{YBCO}} = 12 \times 10^{-6} \text{ K}^{-1}$), a residual strain of approximately 0.45% in the YBCO film can be calculated. This value is very close to the failure limit of 0.5% for compressive strain, as experimentally derived by bending tests in coated conductors.³⁷ To estimate the actual residual strain induced by the Cu substrate in the superconductor, the substrate thickness should be much greater than that of the YBCO film and at least comparable to a typical RABiTs thickness of 50 to 100 μm . For this purpose, we deposited the same buffer layer architecture and YBCO film described in Sec. V on a 1.5-mm-thick Cu crystal. The Cu crystal was nearly a single crystal with a FWHM of 0.28° for the (001) rocking curve and a [001] tilt of 1° . The corresponding FWHMs for the TiN film were 2.57° for the (002) ω -scan and 2.38° for the (111) ϕ -scan. The YBCO showed a $\Delta\omega$ of 2.75° for the (005) peak and a $\Delta\phi$ of 3.65° for the (113) peak. The broadening of the TiN grain alignment with respect to the Cu substrate can be attributed to roughness of the TiN/Cu interface the size of approximately 20 nm over lengths of 1 μm , as shown by cross-section STEM images. As in the case of YBCO films deposited on Cu films, the MgO layer seemed to planarize the TiN features and a very flat interface between YBCO and LMO was observed. The morphology of the YBCO film was consistent with that of high- J_c YBCO films on single-crystal substrates, as shown in the scanning electron microscopy micrograph of Fig. 11. Figure 12 shows a J_c data plot obtained by measuring the

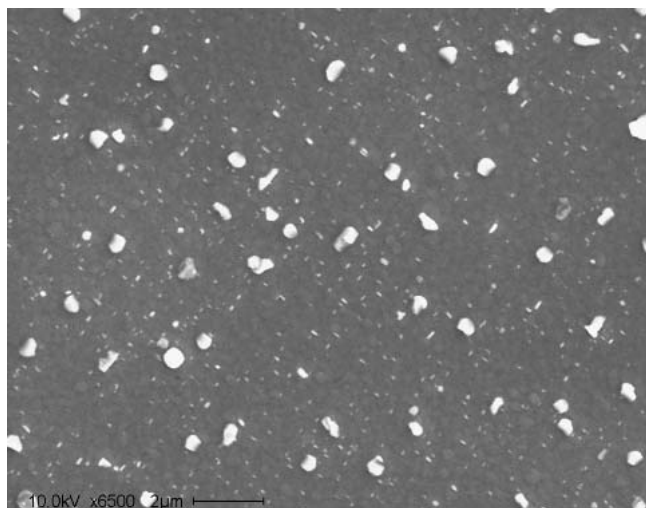


FIG. 11. SEM micrograph of the YBCO film deposited on LMO/MgO/TiN buffer layers on a (001) Cu bulk crystal.

sample magnetic moment hysteresis in a superconducting quantum interference device (SQUID) magnetometer as function of temperature and field. The observed sharp T_c transition and the high value of J_c at low temperature ($J_c[5\text{ K}] = 1.42 \times 10^7\text{ A/cm}^2$) are indicative of absence of weak links. The value of J_c at 77 K and low magnetic field is 1 MA/cm^2 . Quasi-static magnetic measurements probe the current conduction at electric fields two or more orders of magnitude smaller than those used in transport measurements (which generally use a J_c -criterion of $1\text{ }\mu\text{V/cm}$). Therefore, in high- T_c superconductors, in which thermal activation produces a softer electric field-current dependence at low electric fields, magnetic measurements typically yield a lower J_c value than transport measurements by a factor of about 2 to 3, as estimated by our comparisons between the two techniques. According to these observations, and considering that, when measured, the sample had some level of oxygen deficiency (Fig. 13) we can conclude that the J_c at 77 K would be 2 to 3 MA/cm^2 if measured by transport. (Transport measurements require oxygen annealing of the Ag contacts to ensure good contact resistance. Such anneal also ensures full oxygen stoichiometry of the YBCO film. The postanneal step was skipped in this case because magnetic measurements do not require electrical contacts, and the oxygen content of the film therefore resulted from the deposition process itself.) Further, such a value is consistent with the mosaic spread of the YBCO film measured by XRD, according to our previous studies of transport J_c dependence on grain boundary angle in the low-angle regime.³⁸ This result implies that the performance of the YBCO film in this case was not significantly affected by additional, nonintrinsic material issues, including residual strain of the YBCO lattice. By measuring the lattice parameters of the layers composing

our heterostructure, we calculated a lattice distortion of $(a - c)/a = -1.31\%$ in the TiN film and 0.04% for MgO. Figure 13 shows a comparison of YBCO lattice constants as obtained by high-resolution XRD measurements on the present sample, an YBCO sample on Cu film, and an YBCO sample deposited on a high- J_c LMO/MgO-buffered Ni-3%W textured substrate. From these data we deduce that the residual strain in the YBCO film on a Cu substrate is $\epsilon_{zz} = 0.25\%$, in the worse case scenario of a 1.5-mm-thick substrate. This value is significantly lower than the 0.45% estimated on the basis of differences in thermal expansion and close to the residual strain

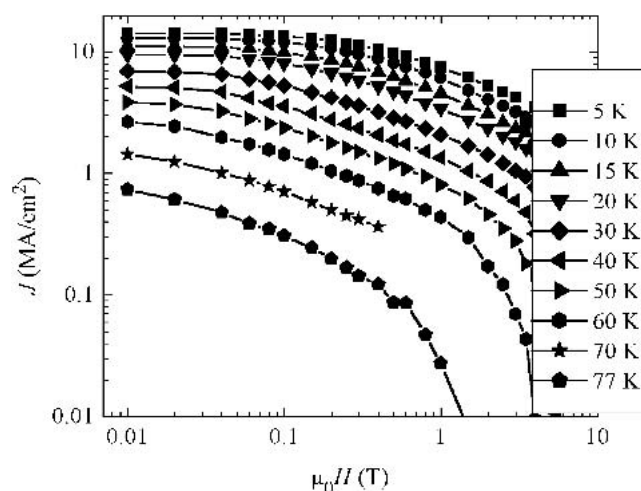


FIG. 12. J_c data versus applied magnetic field at different temperatures for the YBCO film deposited on LMO/MgO/TiN/Cu (crystal) acquired by magnetization hysteresis measurements.

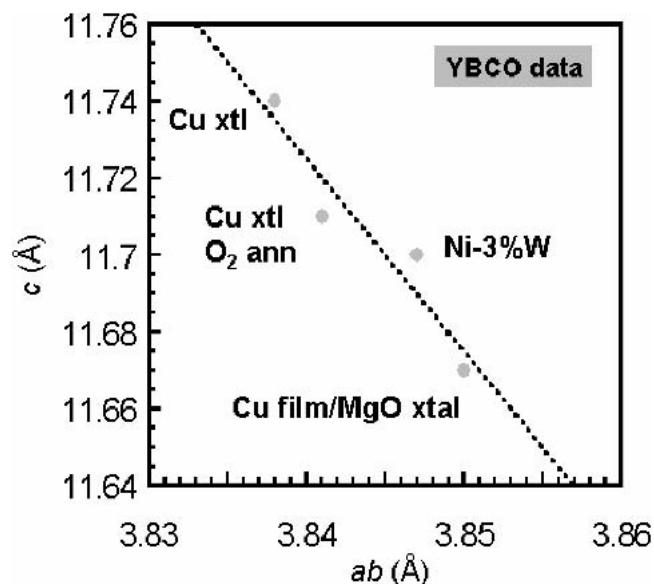


FIG. 13. Out-of-plane versus in-plane lattice constants of YBCO films deposited on the different substrates indicated in the text, measured by high-resolution XRD.

measured on the Ni-3%W substrate. The discrepancy between the calculated and measured value for the YBCO compressive strain indicates that strain-relief mechanisms take place at some level in the buffer layers, as also suggested by STEM observations [Fig. 8(b)].

VII. RESULTS ON {001}<001> TEXTURED Cu TAPES

The experiments performed on Cu films and single crystals were aimed at assessing adequacy of the chosen buffer-layer architecture for deposition of YBCO on biaxially textured Cu tapes. Such experiments showed that the LMO/MgO/TiN multilayered structure is a template

with adequate physical, structural, and mechanical properties for the deposition of laser-ablated YBCO films. The only aspects that our experiments on Cu single crystals do not account for are the influence of the particular surface finishing of the actual textured tapes and the effect of low-angle grain boundaries on the physical and structural properties of the buffer layers.

To complete our study, we grew the LMO/MgO/TiN buffer layer heterostructure, and the YBCO film on 99.99% pure Cu tapes that were thermomechanically processed to obtain a biaxial texture with XRD FWHMs of approximately 6° for in-plane and out-of-plane alignment. Table 1 summarizes the properties of all the different samples discussed in the paper. Figure 14 shows

TABLE I. Summary of the various heterostructures discussed in the text and their properties.

Substrate	Buffer architecture	Thickness (nm)	Texture information	J_c 77 K (A/cm ²)	Comments
Cu/STO	CeO ₂ /YSZ/CeO ₂	50/500/50	45°-rotated cube epitaxy of CeO ₂ on Cu	—	Extensive oxidation/diffusion
Cu/STO	LMO/MgO/STO	300/200/5	Cube-on-cube epitaxy	—	Did not block Cu diffusion
Cu/MgO (or STO)	LMO/MgO/TiN	200/120/160	$\Delta\omega_{\text{YBCO}} = 1.03^\circ$ $\Delta\phi_{\text{YBCO}} = 2.54^\circ$	3.5×10^{6a}	Clean interfaces
Cu crystal	LMO/MgO/TiN	120/80/190	$\Delta\omega_{\text{YBCO}} = 2.75^\circ$ $\Delta\phi_{\text{YBCO}} = 3.65^\circ$	1×10^{6b}	Rough TiN/Cu interface
Textured Cu tape	LMO/MgO/TiN	150/120/200	$\Delta\omega_{\text{LMO}} = 3.73^\circ$ $\Delta\phi_{\text{LMO}} = 6.14^\circ$	0.5×10^{6b}	CuO on rolling marks

^aTransport measurement.

^bMagnetization measurement.

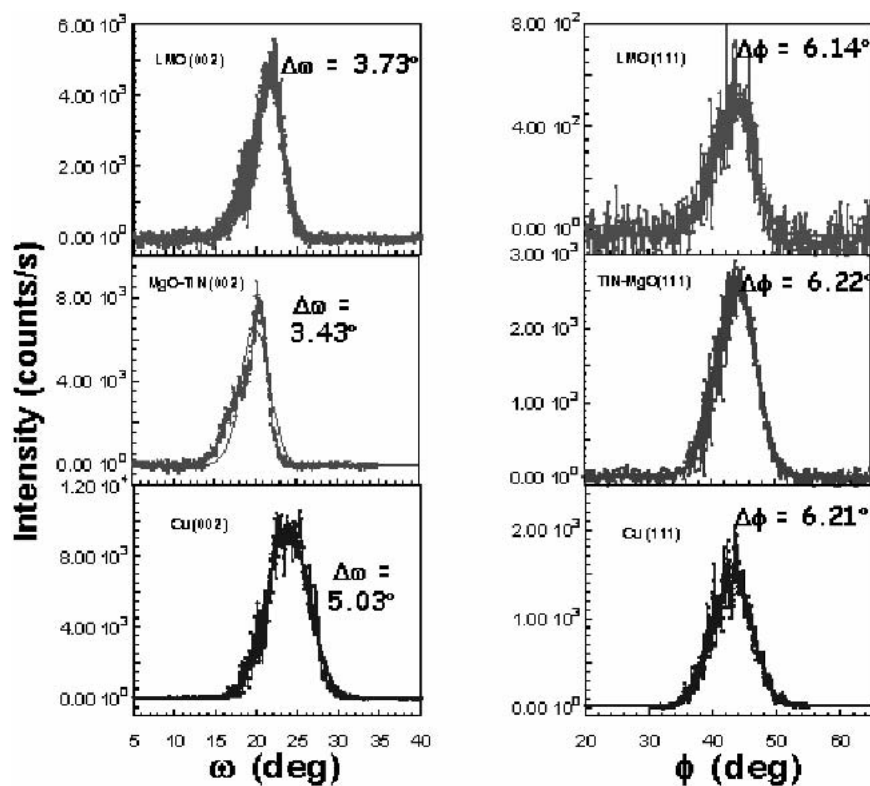


FIG. 14. Omega and phi scans of a biaxially textured Cu tape and the TiN, MgO, and LMO buffer layers epitaxially deposited on it.

the x-ray peaks of selected in-plane and out-of-plane reflections for the Cu substrate and the buffer layers deposited in the same conditions and with the same thickness used for single-crystal Cu samples. We notice that the in-plane texture of the buffer layers reproduces exactly that of the substrate, whereas the out-of-plane texture of the TiN/MgO films is significantly sharper, leading to a sharper grain alignment in the LMO as well. These results differ from those obtained on single-crystal Cu samples, where the TiN film always showed an alignment slightly broader than that of the substrate. If, as we argue in Sec. V., the structural broadening of the TiN films on single-crystal Cu is due to the rough substrate surface, the smoother surface of the textured Cu tape (with an average roughness of only 0.2 nm over areas of $2 \times 2 \mu\text{m}^2$) can be responsible for the higher degree of texture in these films. The sharpening of the out-of-plane distribution is consistent with the “self-planarizing” growth mode of the MgO layer observed in the previous TEM micrographs, but further investigation is needed to understand the mechanism responsible for this phenomenon. Figure 15 shows some J_c data as a function of temperature and magnetic field for an YBCO/LMO/MgO/TiN/ $\{100\}\{100\}$ Cu sample acquired measuring the magnetic hysteresis with a SQUID magnetometer. In this case, the J_c at 77 K and low magnetic field is 0.5 MA/cm^2 , corresponding to a transport J_c value of nearly 1 MA/cm^2 . Although this is a very encouraging value, it is not consistent with the optimal degree of texture of the buffered substrate, which, according to previous studies on the dependence of transport J_c on grain boundary distribution in coated conductors, should correspond to a J_c value nearly two times larger.^{39,40}

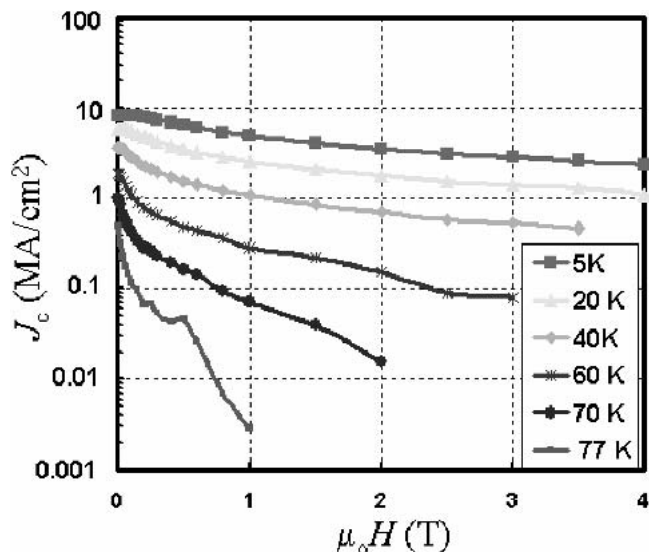
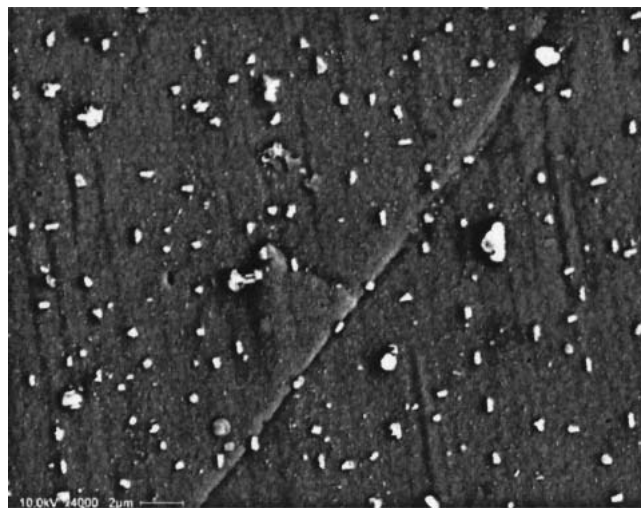


FIG. 15. J_c data versus applied magnetic field at different temperatures acquired by magnetization measurements on a YBCO/LMO/MgO/TiN/Cu (tape) sample.

These samples also showed a lower T_c than typical YBCO films on coated conductors ($T_c = 87.3 \text{ K}$), which suggests the possibility of chemical contamination of the YBCO film by outward Cu diffusion. SEM measurements were consistent with this hypothesis and in particular showed Cu_xO outgrowths in the form of big particles and straight lines aligned with the substrate rolling direction. An example of these features is shown in Fig. 16. From these micrographs, reproduction of rolling features in the YBCO film on the scale of $10 \mu\text{m}$ is also evident. An AFM micrograph of the bare substrate is shown in Fig. 17. As expected, the micrograph reveals linear rolling marks, some of them deeper and decorated by round pits as deep as 25 nm. Such pits could be the result of impurities present on the Cu tape during the



(a)



(b)

FIG. 16. SEM micrographs of the YBCO film deposited on LMO/MgO/TiN/Cu (tape), whose J_c data are reported in Fig. 15.

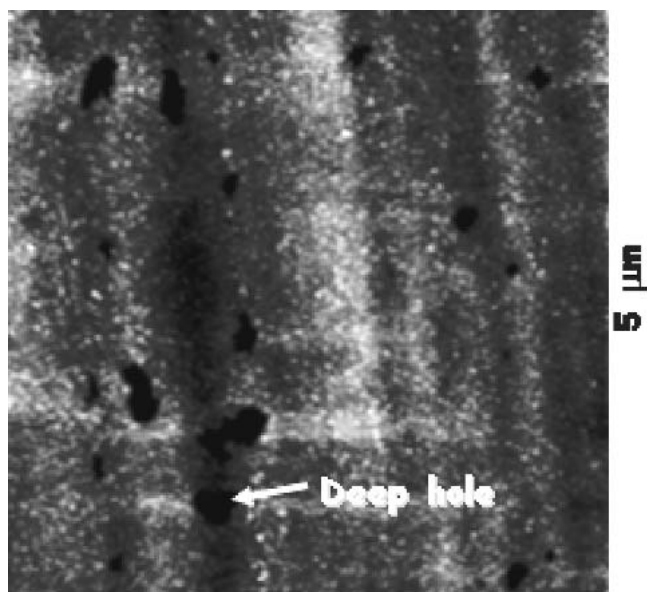


FIG. 17. AFM micrograph of the surface of the textured Cu tape used to deposit the YBCO/LMO/MgO/TiN multilayer structure.

rolling process. It is likely that such features produce highly defective regions in the buffer layers, hindering their performance as a diffusion barrier and ultimately producing the Cu–O outgrowths observed in SEM during the YBCO deposition. At the same time, no such Cu_xO eruptions were observed along the Cu substrate grain boundaries, whose traces are still visible through the YBCO film. A SEM image of such a region is shown in Fig. 16 and suggests very good coverage of the YBCO film across the grain boundary. More controlled experiments on bicrystal substrates are ongoing to address the effect of low-angle TiN grain boundaries on Cu diffusivity.

VIII. CONCLUSIONS

In conclusion, we have demonstrated that a multilayered structure consisting of LMO/MgO/TiN shows all the buffer-layer characteristics of a good diffusion barrier and optimal structural template for the deposition of high- J_c YBCO film on pure Cu substrates. Each of the three buffer layers has a unique property that is essential to suppress Cu oxidation, keep the interfaces clean, accommodate strain, and thus form a high-quality YBCO film on a Cu substrate. TiN is a barrier to outward Cu diffusion, MgO is a barrier to oxygen diffusion and stable enough thermodynamically to be grown on TiN, and LMO provides structural compatibility with the YBCO lattice. It is worth noting that LMO becomes electrically conductive when slightly doped with Sr or Ca. Therefore, electrically conductive buffer-layer architectures for Cu could be fabricated if MgO can be replaced with a conducting oxide having similar properties. This topic will be the subject of future investigation.

We have widely investigated our YBCO/LMO/MgO/TiN/Cu samples by Z-contrast STEM, high-resolution XRD, SEM, RHEED, and AFM. We have addressed many issues involved with the use of Cu substrates for coated conductors, such as Cu diffusivity, Cu oxidation, TiN decomposition in oxygen, differential thermal expansion of Cu and YBCO, residual stress in the YBCO film and the buffer layers, quality and atomic structure of the interfaces, and seed-layer nucleation issues on the Cu surface. Our analysis has revealed that the proposed architecture is an optimal candidate for the development of Cu-based coated conductors that would offer considerable advantages over the present Ni-based coated conductors.

ACKNOWLEDGMENTS

The authors wish to thank P.H. Fleming and Dr. T. Aytug, Oak Ridge National Laboratory-Condensed Matter Science Division (ORNL, CMSD) for depositing Cu films on single-crystal substrates, Dr. A.D. Gapud (ORNL, CMSD) for his help with the J_c transport measurements, and G. Ownby (ORNL, CMSD) for providing and polishing the Cu crystal substrates. This research was sponsored by the U.S. Department of Energy under contract DE-AC05-00OR22725 with the Oak Ridge National Laboratory, managed by UT-Battelle, LLC. One of the authors is a Eugene P. Wigner Fellow and staff member at the Oak Ridge National Laboratory.

REFERENCES

1. A. Goyal, D.P. Norton, J.D. Budai, M. Paranthaman, E.D. Specht, D.M. Kroeger, D.K. Christen, Q. He, B. Saffian, F.A. List, D.F. Lee, P.M. Martin, C.E. Klabunde, E. Hartfield, and V.K. Sikka, *Appl. Phys. Lett.* **69**, 1795 (1996).
2. A. Goyal, E.D. Specht, D.M. Kroeger, and M. Paranthaman, U.S. Patent No. 5 964 966 (12 October 1999).
3. A. Goyal, R. Feenstra, M. Paranthaman, J.R. Thompson, B.W. Kang, C. Cantoni, D.F. Le, F.A. List, P.M. Martin, E. Lara-Curio, C. Stevens, D.M. Kroeger, M. Kowalewski, E.D. Specht, T. Aytug, S. Sathyamurthy, R.K. Williams, and R.E. Ericson, *Physica C* **382**, 251 (2002).
4. W. Prusseit, R. Nemetschek, R. Semerad, B. Holzaphel, and J. Eriquemeyer, Program and extended abstract of the Fifth International Workshop on Superconductivity co-sponsored by ISTE and MRS (Honolulu, Hawaii, 2001), p. 87.
5. V. Boffa, T. Petrisor, C. Annino, F. Fabbri, D. Bettinelli, G. Celentano, L. Ciontea, U. Gambardella, G. Grimaldi, A. Mancini, and V. Galluzi, *Eur. Conf. Appl. Supercond.* (1999).
6. T. Petrisor, V. Boffa, G. Celentano, L. Ciontea, F. Fabbri, U. Gambardella, S. Ceresara, and P. Scardi, *IEEE Trans. Appl. Supercond.* **9**, 2256 (1999).
7. B. de Boer, N. Reger, L. Fernandez G.R., J. Elickemeyer, P. Berberich, W. Prusseit, B. Holzapfel, and L. Schultz, *IEEE Trans. Appl. Supercond.* **11**, 3477 (2001).
8. C.L.H. Thieme, S. Annavarapu, W. Zhang, V. Prunier, L. Fritzemeier, G. Li, U. Schoop, M.W. Rupich, M. Gopal, S.R. Foltyn, and T. Holesinger, *IEEE Trans. Appl. Supercond.* **11**, 3329 (2001).

9. T. Watanabe, Y. Ohashi, M. Ozaki, K. Yamamoto, T. Maeda, K. Wada, and I. Hirabayashi, Program and extended abstracts of the Fifth International Workshop on Superconductivity co-sponsored by ISTECH and MRS (Honolulu, Hawaii, 2001), p. 21.
10. G. Yuan, J. Yang, and K. Shi, *IEEE Trans. Appl. Supercond.* **11**, 3328 (2001).
11. J.R. Thompson, A. Goyal, D.K. Christen, and D.M. Kroeger, *Physica C* **370**, 169 (2002).
12. D.T. Verebelyi, U. Schoop, C. Thieme, X. Li, W. Zhang, T. Kodenkandath, A.P. Malozemoff, N. Nguyen, E. Siegal, D. Buczek, J. Lynch, J. Scudiere, M. Rupich, A. Goyal, E.D. Specht, P. Martin, and M. Paranthaman, *Supercond. Sci. Technol.* **16**, L19 (2003).
13. A. Goyal, D.M. Kroeger, M. Paranthaman, D.F. Lee, R. Feenstra, and D.P. Norton, U.S. Patent No. 6 451 450 (17 September 2002).
14. C. Cantoni, T. Aytug, D.T. Verebelyi, M. Paranthaman, E.D. Specht, D.P. Norton, and D.K. Christen, *IEEE Trans. Appl. Supercond.* **11**, 3309 Part 3 (2001).
15. Y. Fu, O. Tsukamoto, and M. Furse, *IEEE Trans. Appl. Supercond.* **13**, 1780 (2003).
16. S. Mrowec and K. Przybylski, *Oxid. Met.* **6**, 365 (1977).
17. K. Fueki and J.B. Wagner, *J. Electrochem. Soc.* **112**, 384 (1965).
18. S. Mrowec and A. Stoklosa, *Oxid. Met.* **3**, 291 (1971).
19. T.D. Sullivan, in *Stress Induced Phenomena in Metallization*, edited by O. Kraft, E. Arzt, C.A. Volkert, P.S. Ho, and H. Okabayashi, AIP Conference Proceedings No. 491 (1999), pp. 39–50.
20. T. Aytug, A. Goyal, N. Rutter, M. Paranthaman, J.R. Thompson, H.Y. Zhai, and D.K. Christen, *J. Mater. Res.* **18**, 872 (2003).
21. C. Cantoni, D.K. Christen, L. Heatherly, M.M. Kowalewski, F.A. List, A. Goyal, G.W. Ownby, D.M. Zehner, B.W. Kang, and D.M. Kroeger, *J. Mater. Res.* **17**, 2549 (2002).
22. C. Cantoni, D.K. Christen, R. Feenstra, D.P. Norton, A. Goyal, G.W. Ownby, and D.M. Zehner, *Appl. Phys. Lett.* **79**, 3077 (2001).
23. F.A. List and D. Lee, *Continuous Processing and Characterization of Coated Conductors*, presented at the 2002 DOE Peer Review, July 17–19, Washington D.C., available from <http://www.ornl.gov/HTSC/fy02peer.htm>.
24. J.L. Domange and J. Oudar, *Surf. Sci.* **11**, 124 (1968).
25. M.L. Colaianni, P. Syhler, and I. Chorkendorff, *Phys. Rev. B: Condens. Matter* **52**, 2076 (1995).
26. M.L. Colaianni and I. Chorkendorff, *Phys. Rev. B: Condens. Matter* **50**, 8798 (1994).
27. S. Rousset, S. Gauthier, O. Siboulet, W. Sacks, M. Belin, and J. Klein, *Phys. Rev. Lett.* **63**, 1265 (1989).
28. M-H. Yang and C.P. Flynn, *J. Phys.: Condens. Matter* **8**, L279 (1996).
29. P.S. Manning, J.D. Sirman, and J.A. Kilner, *Solid State Ionics* **93**, 125 (1997).
30. C. Cantoni, D.K. Christen, J.R. Thompson, M. Paranthaman, H.Y. Zhai, and A. Goyal (unpublished).
31. I. Kim, P.N. Barnes, A. Goyal, S.A. Barnett, R. Biggers, G. Kozlowski, C. Varanasi, I. Maartens, R. Nekkanti, T. Peterson, T. Haughan, and S. Sambasivan, *Physica C* **377**, 227 (2002).
32. S-Q. Wang, I. Raaijmakers, B.J. Burrow, S. Suthar, S. Redkar, and K-B. Kim, *J. Appl. Phys.* **68**, 5176 (1990).
33. D.P. Norton, A. Goyal, J.D. Budai, D.K. Christen, D.M. Kroeger, E.D. Specht, Q. He, B. Saffian, M. Paranthaman, C.E. Klabunde, D.F. Lee, B.C. Sales, and F.A. List, *Science* **274**, 755 (1996).
34. S.J. Pennycook and P.D. Nellist, in *Impact of Electron and Scanning Probe Microscopy on Materials Research*, edited by D.G. Rickerby, U. Valdré, and G. Valdré (Kluwer Academic, Dordrecht, The Netherlands, 1999), pp. 161–207.
35. A.F. Marshall, K. Char, R.W. Barton, A. Kapitulnik, and S.S. Laderman, *J. Mater. Res.* **5**, 2049 (1990).
36. M. Varela, A.R. Lupini, S.J. Pennycook, Z. Sefrioui, and J. Santamaria, *Solid-State Electron.* (2003, in press).
37. C. Park, D.P. Norton, J.D. Budai, D.K. Christen, D. Verebelyi, and R. Feenstra, *Appl. Phys. Lett.* **73**, 1904 (1998).
38. D.T. Verebelyi, C. Cantoni, J.D. Budai, D.K. Christen, H.J. Kim, and J.R. Thompson, *Appl. Phys. Lett.* **78**, 2031 (2001).
39. D.T. Verebelyi, D.K. Christen, R. Feenstra, C. Cantoni, A. Goyal, D.F. Lee, M. Paranthaman, P.N. Arendt, R.F. De Paula, J.R. Groves, and C. Prouteau, *Appl. Phys. Lett.* **76**, 1755 (2000).
40. R. Feenstra, *Ex-Situ Growth of YBCO Thick Films by the BaF₂ Process*, presented at the 2002 DOE Peer Review on high-*T_c* superconductivity, Washington D.C., July 2002, available from <http://www.ornl.gov/HTSC/fy02peer.htm>.